

Cross-correlation studies as a probe of reionization physics

Anže Slosar^{1,2}, Asantha Cooray³, Joseph I. Silk¹

¹*Oxford Astrophysics, Denys Wilkinson Building, Keble Road, OX13RH, Oxford, United Kingdom*

²*Faculty of Mathematics and Physics, University of Ljubljana, Slovenia*

³*Center for Cosmology, Department of Physics and Astronomy, University of California, Irvine, CA 9269, USA*

Accepted —; received —; in original form 15 May 2018

ABSTRACT

The process of reionization is now believed to have proceeded in an orchestrated manner beginning with UV photons emitted by high redshift galaxies containing a large fraction of Population III stars carving out ionised regions around them. The physics during this era can be studied with a combination of redshifted 21-cm spin-flip transition tracing neutral hydrogen gas, IR emission from massive primordial stars that trace the global star-formation rate during reionization, and the imprint of hot-electrons in first supernovae remnants Compton-cooling off of cosmic microwave background (CMB) radiation through the Sunyaev-Zel’dovich effect. While these individual effects and their observable signatures have been advocated as probes of reionization history, here we show how cross-correlation studies between these signals can be used to further understand physics during reionization. Cross-correlation studies are advantageous since the measurable statistics do not suffer in the same manner from foregrounds and systematic effects as is the case of auto-correlation function measurements. We discuss the prospects for detecting various cross-correlation statistics using present and next generation experiments and the information related to reionization captured by them.

Key words: cosmology: theory — large scale structure — infrared: general — stars: formation — cosmology: observations — diffuse radiation

1 INTRODUCTION

The 21-cm spin-flip transition of neutral Hydrogen, either in the form of an absorption or an emission relative to Cosmic Microwave Background (CMB) blackbody spectrum, provides one of the best ways to study the intergalactic medium during and prior to reionization (Scott & Rees 1990; Tozzi et al. 2000; Madau et al. 1997; Furlanetto et al. 2004; Santos & Cooray 2006). With frequency selection for observations, the 21-cm line, in principle, provides three-dimensional tomography of the reionization era as well as a probe to the dark ages where no luminous sources are present. The exact physics associated with the reionization process is still largely unknown, though it is strongly believed that UV photons from first luminous sources are responsible for it (Barkana & Loeb 2001; Furlanetto et al. 2006). These UV photons create bubbles (Wyithe & Loeb 2003; Cen 2003a,b; Haiman & Holder 2003; Mackey et al. 2003; Santos et al. 2003; Yoshida et al. 2003, 2004; Zahn et al. 2006) of ionised material around them, although it is still unclear whether densest or least-dense regions were ionised first (Furlanetto & Oh 2005; Cohn & Chang 2006). Direct detection of auto-correlation spectra of this signal might prove to be difficult, due to very strong foregrounds, although various cleaning

techniques have been proposed (Zaldarriaga et al. 2004; Santos et al. 2005; Morales et al. 2006)

The same reionization redshifts can also be probed at near-IR wavelengths since the intensity of the cosmic near-infrared background (IRB) is a measure of the total light emitted by stars and galaxies in the Universe. The possibility that there is a high-redshift component to the IRB comes from the fact that the absolute background estimated by space-based experiments, such as the Diffuse Infrared Background Experiment (DIRBE; Hauser & Dwek (2001)) and the Infra-Red Telescope in Space (IRTS; Matsumoto et al. (2005)), is significantly larger than the background accounted for by resolved sources so far: only 13.5 ± 4.2 nW m⁻² sr⁻¹ is resolved to point sources at 1.25 μ m (Cambrésy et al. 2001), while current direct measurements range from 25-70 nW m⁻² sr⁻¹ (see Kashlinsky (2006) for a recent review).

Primordial galaxies at redshifts 8 and higher, especially those involving Population III stars, are generally invoked to explain the missing IR flux between 1 μ m and 2 μ m, with most of the intensity associated with redshifted Lyman- α emission during reionization (Santos et al. 2002; Salvaterra & Ferrara 2003; Cooray & Yoshida 2004; Fernandez & Komatsu 2006). While models of high-redshift Pop III popula-

tions can explain the “missing” IRB, these models run into several difficulties if such sources were to account for all of the missing IR intensity. These include the high efficiency required to convert baryons to stars in first galaxies (see e.g. Madau & Silk 2005) and limits from deep IR imaging data that suggest a lack of a large population of high-redshift dropouts (Salvaterra & Ferrara 2006). Still, one does expect some contribution to the IRB from sources that reionized the Universe, though the exact intensity of the IRB from such sources is yet unknown both theoretically and observationally.

As pointed out in Cooray et al. (2004) (see also Kashlinsky et al. 2004), if a high-redshift population contributes significantly to the IRB, then these sources are expected to leave a distinct signal in the anisotropy fluctuations of the near-IR intensity, when compared to the anisotropy spectrum associated with low-redshift sources. Such a study has been attempted with anisotropy measurements using Spitzer data with preliminary indications for an excess anisotropy in the background at arcminute angular scales and below (Kashlinsky et al. 2005). There are, however, large uncertainties on the exact fraction of IRB intensity from redshifts during reionization (Sullivan et al. 2006; Salvaterra et al. 2006), especially given the suggestions that these excess IRB fluctuations can be partly explained with expected clustering from faint unresolved galaxies in optical images but not present in IR images (Cooray et al. 2006). Here, we suggest that an approach to establish the presence of IRB anisotropies from the era of reionization, such as those due to first-stars, will be to consider a cross-correlation of the IRB against brightness temperature fluctuations in the 21-cm background.

Finally, the small-scale cosmic microwave background (CMB) anisotropies are also expected to contain signatures from the reionization epoch (Santos et al. 2003; Zahn et al. 2005; McQuinn et al. 2006, 2005; Alvarez et al. 2006). Uniquely identifying the fractional anisotropy contribution from reionization era is challenging with CMB data alone since a large number of sources contribute to the anisotropies of CMB at arcminute angular scales and below. These include thermal Sunyaev-Zel’dovich (SZ) effect from low-redshift galaxy clusters, the Ostriker-Vishniac effect associated with bulk motions of the electron density field, and gravitational lensing modifications to CMB anisotropies. In terms of reionization contributions, one expects an anisotropy when electrons in the surrounding medium of first supernovae explosions Compton-cool against the CMB (Oh et al. 2003); the modification to CMB is similar to the y -distortion related to SZ scattering in clusters. Such a signal need not be associated with supernovae alone, as X-rays from first quasars, supernovae, and star clusters are also expected to heat the intergalactic medium (IGM) at high redshifts (Oh 2001; Venkatesan et al. 2001). Such a high-redshift contribution could also help explain the excess CMB anisotropy at arcminute angular scales, as seen by CBI (Mason et al. 2003), BIMA (Dawson et al. 2002; Dawson et al. 2006), and ACBAR (Kuo et al. 2004; Kuo et al. 2006) experiments.

If a high-redshift SZ contribution exists, an interesting possibility to identify it involves the cross-correlation between small-scale CMB anisotropy maps and the 21-cm signal. If the IGM is heated to a temperature above the CMB,

as due to X-ray heating, then the 21-cm signal will be detectable as an emission. While SZ originates from the ionized electrons and the 21-cm signal is related to the neutral Hydrogen distribution, with partial reionization, one expects the two signals to spatially anti-correlate as the regions containing free-electrons trace the same underlying density field defined by dark matter that also leads to fluctuations in the neutral Hydrogen. The cross-correlation between arcminute-scale CMB and the 21-cm can be used to measure the angular power spectrum of this (anti)-correlation and help establish the fraction of SZ effect originating from high-redshifts.

In this paper, we discuss several cross-correlations involving 21-cm data and tracers of reionization discussed above. Since 21-cm observations can be preselected based on the choice of a frequency bin corresponding to the redshifted line emission, one can consider the correlation as a function of the redshift bin and use that information to establish the redshift dependence of the high-redshift SZ signal as well as the IRB component related to primordial galaxies. Here, we discuss the measurement of the proposed cross-correlations using CMB maps from upcoming missions and maps of the IRB from wide-field images. A cross-correlation of the 21-cm signal with galaxy surveys has been discussed in Furlanetto & Lidz (2006) and Wyithe & Loeb (2006).

In this paper we use a simple analytic model to calculate and understand the qualitative features of the cross-correlation. For more accurate quantitative predictions, one should use the numerical simulations, which have recently made significant advances (Iliev et al. 2006a; Mellema et al. 2006; Iliev et al. 2006b; Kohler et al. 2005; Zahn et al. 2006).

This paper is organized as following. In Section 2, we present our basic model for the auto- and cross-correlations of various fields discussed here. In Section 3, we consider a physical model of reionization and discuss our results and observability of various statistics. Finally, we conclude with a summary of our results in Section 5.

2 METHOD

In this Section, we develop simple models for 21cm, high-redshift SZ, and IR backgrounds and their cross-correlation. To describe the 21-cm background, we closely follow the formalism developed in Zaldarriaga et al. (2004) and extend it to encompass the IR and SZ fluctuations as well. The basic starting premise is that the 21-cm fluctuations are tracing the dimensionless brightness temperature field

$$\psi(\hat{\mathbf{n}}, r) = (1 + \delta)x_H, \quad (1)$$

where δ is the fraction over-density and x_H is the neutral fraction, while the IR and SZ fluctuations trace the “sources” field

$$\phi(\hat{\mathbf{n}}, r) = (1 + \delta_s). \quad (2)$$

If we assume that during reionization, the early sources form bubbles of nearly completely ionised gas so that x_H is strongly bimodal and that this gas is everywhere hot enough to produce SZ fluctuations and that it is filled with primordial sources emitting in (observed-frame) infrared light, then it is reasonable to expect that $\phi(\hat{\mathbf{n}}, r) \propto (1 + \delta)x_S$ with $x_S = 1 - x_H$. Here we take a marginally more realistic model, by assuming that sources occupy just some central fraction

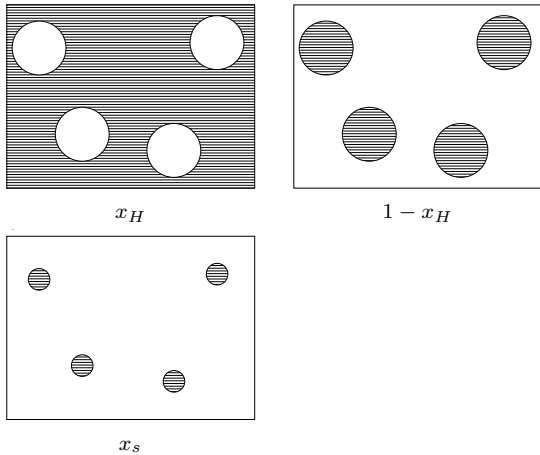


Figure 1. This figure shows schematically, the neutral fraction field x_H (top left), the “negative” neutral fraction field (top right) and the sources field x_s (bottom) used in this paper.

of the reionization halos as illustrated in the Figure 1. To what extent this is a plausible approximation remains to be seen, but it is a useful starting point for the cross-correlation study we propose here.

We will use superscripts n , i , y to describe the 21-cm spin flip transition, i for the IR signal and y for the SZ signal from the epoch of reionization. For example, C_ℓ^{ni} denotes the angular cross-correlation power spectrum between the 21-cm and the IR signals. We will adopt units of mK for the 21-cm signal, nW/m²/sr for the IR signal and the observed μ K decrement in the Rayleigh-Jeans region for the Comptonization parameter (y). The latter is given by $\Delta T = -2T_{\text{CMB}}y$.

Through the paper we use a standard flat cosmology with $\Omega_b = 0.05$, $\Omega_m = 0.3$, $\Omega_\Lambda = 0.7$, $\sigma_8 = 0.8$ and $n_s = 1$, where the symbols have their standard meaning.

2.1 21cm background and power spectrum

In the limit of no redshift distortions and spin temperature of hydrogen being much larger than the CMB temperature, the observed brightness temperature on the sky is given by (Zaldarriaga et al. 2004)

$$T(\hat{\mathbf{n}}) = T_0(r_0) \int dr W(r) \psi(\hat{\mathbf{n}}, r), \quad (3)$$

where $W(r)$ is the window function describing the instrumental bandwidth around some target redshift r_0 , normalized such that $\int dr W(r) = 1$ and

$$T_0(r) = 23\text{mK} \left(\frac{\omega_b}{0.02} \right) \left(\frac{\omega_m}{0.15} \right)^{-1/2} \left(\frac{1+z}{10} \right), \quad (4)$$

with ψ being defined in equation (1)

If we expand ψ in Fourier series

$$\psi(\mathbf{x}) = \int \frac{d^3k}{(2\pi)^3} \psi_k(\mathbf{k}) e^{i\mathbf{k}\cdot\mathbf{r}} \quad (5)$$

and then use the spherical harmonic decomposition of the observed temperature

$$a_{\ell m} = 4\pi i^\ell \int \frac{d^3k}{(2\pi)^3} \psi_k(\mathbf{k}) \alpha_\ell(k, \nu) Y_{\ell m}^*(\mathbf{k})$$

$$\alpha_\ell(k, \nu) = T_0(r_0) \int dr W(r) j_\ell(kr), \quad (6)$$

we can define the angular power spectrum

$$\langle a_{\ell m} a_{\ell' m'}^* \rangle = \delta_{\ell\ell'} \delta_{mm'} C_\ell^{nn}, \quad (7)$$

so that

$$C_\ell^{nn} = 4\pi \int \frac{dk}{k} \Delta_{\psi\psi}^2(k) \alpha_\ell^2(k), \quad (8)$$

where

$$\Delta_{\psi\psi}^2(k) = \frac{k^3}{2\pi^2} P_{\psi\psi}(k) = \frac{k^3}{2\pi^2} \delta^D(\mathbf{k} + \mathbf{k}') \langle \psi_k(\mathbf{k}) \psi_k(\mathbf{k}') \rangle \quad (9)$$

2.2 IR background and power spectrum

We now repeat the exercise for the IR flux from the first stars. The specific intensity is given by

$$I_\nu(\hat{\mathbf{n}}) = \int dr \frac{dI_\nu}{dr} \phi(\hat{\mathbf{n}}, r), \quad (10)$$

with

$$\frac{dI_\nu}{dr} = \frac{1}{\bar{\phi}(r)} \frac{dV}{dr} \Psi(r) t_* \frac{l_*(\nu(1+z))(1+z)}{4\pi D_l^2}, \quad (11)$$

where $\bar{\phi}(r)$ is the average value of ϕ (defined in equation (2)) at a given distance from the observer. Other quantities take care of producing the correct mean intensity: Ψ is the star-formation rate per unit volume at a given redshift, $t_* \sim 5 \times 10^6$ yr, l_* is the mean spectrum per unit mass of a Pop III star and D_l is the luminosity distance. We take the spectrum of first stars from Santos et al. (2002) assuming unity escape fraction. Assuming a different escape fraction would change our results, but quantitatively they would remain the same.

In Figure 2, we plot intensity spectra for a $100 M_\odot$ mass star at redshift of $z = 15$, but observed today. Note the pronounced (even with a logarithmic scale!) Lyman-alpha peak (due to collisionally excited atoms, see Santos et al. (2002)) at around few microns in wavelength. At lower wavelengths, this emission dominates the total intensity signal from such a star. This means that if our observing wavelength is such that the integral includes a contribution from the peak, then the resulting intensity power spectrum would be dominated by this emission.

If we expand ϕ in Fourier series and use the spherical harmonic decomposition in exact analogy with equations (5)–(8) we can define the angular power spectrum given by

$$C_\ell^{ii} = 4\pi \int \frac{dk}{k} \Delta_{\phi\phi}^2(k) \beta_\ell^2(k), \quad (12)$$

where

$$\beta_\ell(k, \nu) = \int dr \frac{dI_\nu(r)}{dr} j_\ell(kr) \quad (13)$$

and

$$\Delta_{\phi\phi}^2(k) = \frac{k^3}{2\pi^2} P_{\phi\phi}(k) = \frac{k^3}{2\pi^2} \delta^D(\mathbf{k} + \mathbf{k}') \langle \phi_k(\mathbf{k}) \phi_k(\mathbf{k}') \rangle \quad (14)$$

2.3 High-redshift SZ component

The high-redshift SZ component is handled in a very similar manner. We write the total Comptonization parameter as

$$y(\hat{\mathbf{n}}) = \int dr \frac{dy}{dr} \phi(\hat{\mathbf{n}}, r). \quad (15)$$

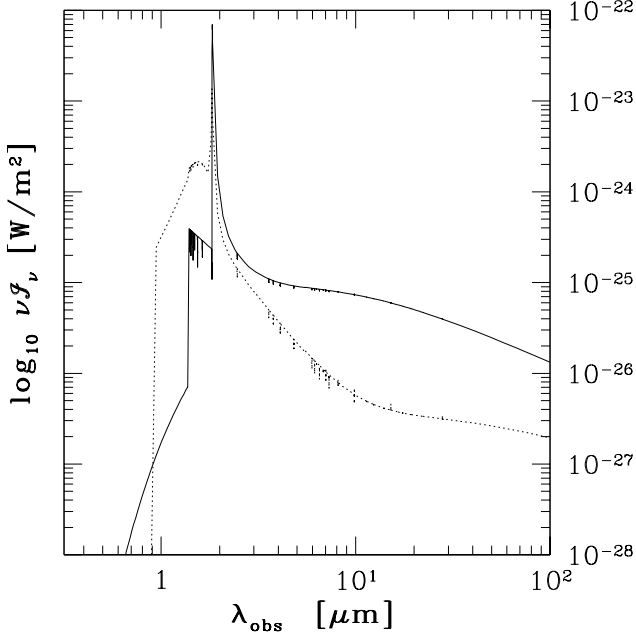


Figure 2. The observed spectrum of 100 solar mass primordial Pop-III star at redshift of $z = 15$ as a function of the observed wavelength. The solid line is for unity escape fraction and the dotted line is for zero escape fraction - see (Santos et al. 2002) for details.

To calculate the Comptonization parameter, we model each supernovae as a spherical ball of radius R . The mean Comptonization parameter per SN remnant is $y = k_b T_e / (m_e c^2) \sigma_T n_e 4R/3$ (σ_T is the Thomson scattering cross-section, m_e is the electron mass) and each remnant contributes over $\pi(R/D_A)^2$ per steradian to mean \bar{y} . Assuming that SN energy $E_{\text{sn}} \sim 10^{44} \text{ J}$ is evenly distributed between electrons ($E_{\text{sn}} = N_e k_b T_e$) one arrives at

$$\frac{dy}{dr} = \frac{1}{\phi(r)} \frac{dV}{dr} \eta_{\text{sn}} \frac{\Psi}{M_{\text{prog}}} t_{\text{sn}} \left(\frac{E_{\text{sn}}}{m_e c^2} \right) \left(\frac{\sigma_T}{D_A^2} \right), \quad (16)$$

where $M_{\text{prog}} \sim 50 M_\odot$ is a typical progenitor mass, and $\eta_{\text{sn}} \sim 0.5 - 1$ takes into account the fact that not all stars end with a supernovae and that not all energy is deposited into hot electrons.

We can now define the angular power spectrum given by

$$C_\ell^{yy} = 4\pi \int \frac{dk}{k} \Delta_{\psi\psi}^2(k) \gamma_\ell^2(k), \quad (17)$$

where

$$\gamma_\ell(k) = \int dr \frac{dy(r)}{dr} j_\ell(kr). \quad (18)$$

2.4 The cross-correlation power spectrum

When cross-correlating with the 21-cm, the cross-correlation power spectra are now defined in exactly the same manner:

$$C_\ell^{ni} = 4\pi \int \frac{dk}{k} \Delta_{\psi\phi}^2(k) \alpha_\ell(k) \beta_\ell(k) \quad (19)$$

$$C_\ell^{ny} = 4\pi \int \frac{dk}{k} \Delta_{\psi\phi}^2(k) \alpha_\ell(k) \gamma_\ell(k) \quad (20)$$

$$C_\ell^{iy} = 4\pi \int \frac{dk}{k} \Delta_{\phi\phi}^2(k) \beta_\ell(k) \gamma_\ell(k) \quad (21)$$

where

$$\Delta_{\psi\phi}^2(k) = \frac{k^3}{2\pi^2} P_{\psi\phi}(k) = \frac{k^3}{2\pi^2} \delta^D(\mathbf{k} + \mathbf{k}') \langle \psi(\mathbf{k}) \phi(\mathbf{k}') \rangle, \quad (22)$$

is the three-dimensional cross-correlation between 21-cm brightness temperature and source fields. In above, indices i , n and y represent anisotropies in the IR, 21-cm brightness temperature (neutral Hydrogen), and the CMB (due to SZ y -parameter), respectively.

3 CROSS-CORRELATION CALCULATION

To proceed, we need to produce a model of correlations of the neutral fraction. If we assume that a) bubbles are uncorrelated and b) that any pocket of gas is either completely ionised or completely neutral, then a good model is (Zaldarriaga et al. 2004)(see also Furlanetto et al. 2004)

$$\langle x_H(\mathbf{x}) x_H(\mathbf{x}') \rangle = \bar{x}_H^2 + (\bar{x}_H - \bar{x}_H^2) f(r/R_b), \quad (23)$$

where $r = |\mathbf{x} - \mathbf{x}'|$, R is typical (or effective) bubble size, $f(x)$ goes to unity at zero and to zero at infinity. So defined auto-correlation function has the desired property that $\langle x_H(\mathbf{x}) x_H(\mathbf{x}') \rangle \rightarrow \bar{x}_H^2$ as $r \rightarrow \infty$ (bubbles are uncorrelated!) and $\langle x_H(\mathbf{x}) x_H(\mathbf{x}') \rangle \rightarrow \bar{x}_H$ as $r \rightarrow 0$ (because x_H is either 1 or 0).

Similarly, the auto-correlation of the x_S field satisfies

$$\langle x_S(\mathbf{x}) x_S(\mathbf{x}') \rangle = \bar{x}_S^2 + (\bar{x}_S - \bar{x}_S^2) f(r/R_s), \quad (24)$$

with the condition that $\bar{x}_S = (1 - \bar{x}_H)(R_s/R_b)^3$ (see Figure 1). To calculate the cross-correlation correctly, one would need to calculate it given function form of $f(x)$. Here we approximate it with one that has correct limits, i.e.

$$\langle x_H(\mathbf{x}) x_S(\mathbf{x}') \rangle = (\bar{x}_S \bar{x}_H) [1 - f(r/R_{bs})]. \quad (25)$$

In this calculation we have simply assumed a constant bubble size of $R_b = 4 \text{ Mpc}/h$ with sources size $R_s = 2 \text{ Mpc}/h$ and the cross-correlation size $R_{bs} = 2.25 \text{ Mpc}/h$.

We can now calculate auto and cross correlators of ψ and ϕ . These are given by

$$\begin{aligned} \langle \psi(\mathbf{x}) \psi(\mathbf{x}') \rangle - \langle \psi \rangle^2 &= [\bar{x}_H^2 + (\bar{x}_H - \bar{x}_H^2) f(r/R_b)] \zeta(r) + \\ &(\bar{x}_H - \bar{x}_H^2) f(r/R_b) + \eta_H(r) [2\bar{x}_H + \eta_H(r)] \end{aligned} \quad (26)$$

$$\begin{aligned} \langle \phi(\mathbf{x}) \phi(\mathbf{x}') \rangle - \langle \phi \rangle^2 &= [\bar{x}_S^2 + (\bar{x}_S - \bar{x}_S^2) f(r/R_s)] \zeta(r) + \\ &(\bar{x}_S - \bar{x}_S^2) f(r/R_s) + \eta_S(r) [2\bar{x}_S + \eta_S(r)] \end{aligned} \quad (27)$$

$$\begin{aligned} \langle \psi(\mathbf{x}) \phi(\mathbf{x}') \rangle - \langle \psi \rangle \langle \phi \rangle &= [(\bar{x}_H \bar{x}_S) (1 - f(r/R_{bs})) \zeta(r) - \\ &(\bar{x}_H \bar{x}_S) f(r/R_{bs}) + \bar{x}_H \eta_S(r) + \bar{x}_S \eta_H(r) + \eta_H \eta_S(r)] \end{aligned} \quad (28)$$

where $\eta_{H,S}$ is the cross-correlation between neutral fraction and density $\eta_{H,S}(r) = \langle \delta(\mathbf{x})x_{H,S}(\mathbf{x}') \rangle$ and ζ is the density contrast correlation function $\zeta(r) = \langle \delta(\mathbf{x})\delta(\mathbf{x}') \rangle$.

Assuming $\eta = 0$, we can now Fourier transform these to obtain the relevant power spectra:

$$P_{\psi\psi}(k) = \bar{x}_H^2 P(k) + (\bar{x}_H - \bar{x}_H^2)(P_{f\delta}(k) + P_f(k)) \quad (29)$$

$$P_{\phi\phi}(k) = (\bar{x}_S)^2 P(k) + (\bar{x}_S - \bar{x}_S^2)(P_{f\delta}(k) + P_f(k)) \quad (30)$$

$$P_{\psi\phi}(k) = (\bar{x}_H \bar{x}_S)(P(k) - P_{f\delta}(k) - P_f(k)), \quad (31)$$

$$(32)$$

where $P_f(k)$ is the Fourier transform of $f(r)$, using the appropriate radius R_b , R_s or R_{bs} and $P_{f\delta}$ is the Fourier transform of $f\xi$.

Finally, we take the highly biased nature of primordial sources into account heuristically by using a biasing factor. The mean bias is given by

$$\bar{b} = \frac{\int_{M_{\min}}^{\infty} dM dN/dMM b(M, z)}{\int_{M_{\min}}^{\infty} dM dN/dMM} \quad (33)$$

We multiply the linear power spectrum by \bar{b}^2 for IR and SZ and their cross-correlation spectra and by the $\bar{b}(z)$ for the cross power spectra of 21cm with either IR or SZ signals. A technically more correct way of performing this calculation would be to correctly take into account the cross-correlation field η .

We use the linear bias function (we take the simple linear bias of Mo & White (1996)) and M_{\min} is the minimal mass corresponding to halos of virial temperature of 2×10^4 K.

3.1 Star-formation history and reionization

To complete our calculation, we need to also specify the star-formation rate and reionization history. In early universe, massive enough halos accrete and cool gas to form stars. A halo of mass M converts a fraction of $f_* f_b$ of its mass into first massive stars that later explode as supernovae, where $f_* \sim 0.2$ is the fraction of baryons that fragment to form stars and $f_b = \Omega_b/\Omega_m \approx 0.2$ is the baryon fraction.

The total density in stars at any redshift is given by

$$\rho_*(z) = \int_{M_{\min}}^{\infty} \rho_*(M, z) dM = \int_{M_{\min}}^{\infty} f_* f_b M \frac{dN}{dM} dM, \quad (34)$$

where dN/dM is the number density of halos per unit mass range. We take the Press-Schechter (Press & Schechter 1974) form of the number counts. The star-formation rate per comoving volume for halos with mass between M and $M+dM$ is then simply

$$\Psi(M, z) = \frac{d}{dt} \rho_*(M, z) = \frac{dz}{dt} \frac{d}{dz} \rho_*(M, z) \quad (35)$$

with

$$\frac{dz}{dt} = H_0(1+z) (\Omega_m(1+z)^3 + \Omega_k(1+z)^2 + \Omega_\Lambda)^{1/2} \quad (36)$$

We can also make a very simple model that connects the reionized fraction and star-formation activity. If we take a steady-state approximation and assume that $q \sim 4000$ ionizing photons are emitted per baryon in stars, then the

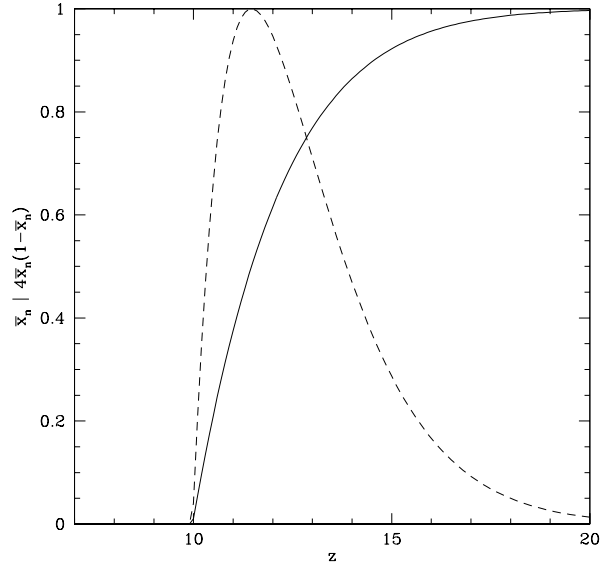


Figure 3. The neutral fraction (\bar{x}_H) as a function of redshift as estimated by the equation (37). The dashed line shows the $4\bar{x}_H(1-\bar{x}_H)$ – a quantity that is directly proportional to amplitude of cross-correlation power spectra.

ionised fraction is simply given by

$$1 - \bar{x}_H = \min \left[\frac{qt_{\text{rec}}}{\Omega_b \rho_{\text{crit}}} \frac{d\rho_*}{dt}, 1 \right], \quad (37)$$

where the recombination time scale is given by Madau et al. (1999)

$$t_{\text{rec}} = 0.3 \left(\frac{\omega_b}{0.02} \right)^{-1} \left(\frac{1+z}{4} \right)^{-3} \left(\frac{C}{30} \right)^{-1} \quad (38)$$

where we assumed the clumping factor $C = \langle n_{\text{HII}}^2 \rangle / \langle n_{\text{HII}} \rangle^2 \sim 50$. The resulting neutral fraction is plotted in the Figure 3.

3.2 Approximations

Two common approximations are used in the calculation of power spectra, depending on the ratio of survey depth compared to the angular scales of interest. If $\delta r / (D_A \ell^{-1}) \ll 1$, then window function can be approximated as a delta function and the equation (8) reduces to

$$C_\ell^{nn} = 4\pi T_0(r_0)^2 \int \frac{dk}{k} \Delta_{\psi\psi}^2(k) j_\ell^2(kr_0), \quad (39)$$

and equivalent for equations (12) and (19).

The other limit is when $\delta r / (D_A \ell^{-1}) \gg 11$ one can use the so-called Limber approximation:

$$\int dk F(k) j_\ell(kr_1) j_\ell(kr_2) \approx \frac{\pi}{2r_1^2} \delta(r_1 - r_2) F(\ell/r_1) \quad (40)$$

The necessary condition is that $F(k)$ is a smoothly varying function. When applied to the power spectra, this results in equation (8) simplifying to

$$C_\ell^{nn} = \int dr (T_0(r) W(r))^2 P(\ell/d_A) r^{-2}. \quad (41)$$

If additionally $\delta r \ll r$, one can simply further to

$$C_\ell^{nn} = T_0^2(r) P(\ell/d_A) r^{-2} (\delta r)^{-1}, \quad (42)$$

where δr is the effective width of the windows function $W(r)$. Analogous expressions hold for other equations for cross-correlation spectra are:

$$C_\ell^{ni} = T_0(r) \frac{dI_\nu}{dr(r)} P(\ell/d_A) r^{-2}, \quad (43)$$

$$C_\ell^{ny} = T_0(r) \frac{dy}{dr(r)} P(\ell/d_A) r^{-2}. \quad (44)$$

The interesting point here is that the auto-correlation power spectrum in units of temperature scales inversely with bandwidth (δr), while the cross-correlation power spectra are, in the Limber limit, to first order independent of it.

In Figure 4, we plot a sample spectrum using the full formula (8) and the two approximations in equations (39) and (42). We obtain the expected result: for narrow bandwidths and large angular scales the delta function approximation fares better, but for bigger bandwidths the Limber approximation is more appropriate. The unexpected discrepancy at large bandwidths and small scales is likely due to ringing of the window function, which does not seem to cancel out completely as assumed in the Limber approximation.

4 RESULTS

The auto-correlation power spectra of our model are comparable with published results. We plot some of them, together with some published data in the Figure 5. The observational uncertainties in the parameters of our model give an overall uncertainty in the amplitude of the signal of about order of magnitude. The mean Comptonization parameter in our model is $\bar{y} = 5 \times 10^{-6}$, which is compatible with the COBE-FIRAS upper limit around at the same level (Mather et al. 1994). The $2\mu\text{m}$ mean IR flux from first sources during reionization $\sim 5 \text{ nW m}^{-2} \text{ sr}^{-1}$ an $2\mu\text{m}$, which is within experimental upper limits on the IRB intensity (about 20 to 70 $\text{nW m}^{-2} \text{ sr}^{-1}$) at those wavelengths (Cambr sy et al. 2001).

In Figure 6 we plot the relative cross-correlation coefficient $C_\ell^{ni} / \sqrt{C_\ell^{ii} C_\ell^{nn}}$ for the cross-correlation of the 21cm and the IR signals. We naturally expect a negative cross-correlation between the red-shifted 21-cm signal and the infrared light from the stars. Even in our simplified model this anti-correlation does not hold on large scales where the signal is dominated by the density perturbations that correlate positively. The cross-over scale correspond to the typical size of the bubbles. Therefore, we generically predict that IR and 21-cm line signals to be correlated on large scale and anti-correlated on small scales. The cross-over scale can be used to determine the typical size of the bubbles. Our calculations are probably accurate to only an order of magnitude, but the heuristics should nevertheless be robust. Secondly, we note that when small enough ($\sim 2\mu\text{m}$) wavelength is used, then the IR signal is dominated by a rather narrow redshift range and the cross-correlation will be picked only when 21-cm observation are tuned to the same redshift range. When observing the continuum radiation at larger wavelengths, the cross-correlation is much less pronounced, but present at all redshifts. In Figure 7 we plot the same for cross-correlating

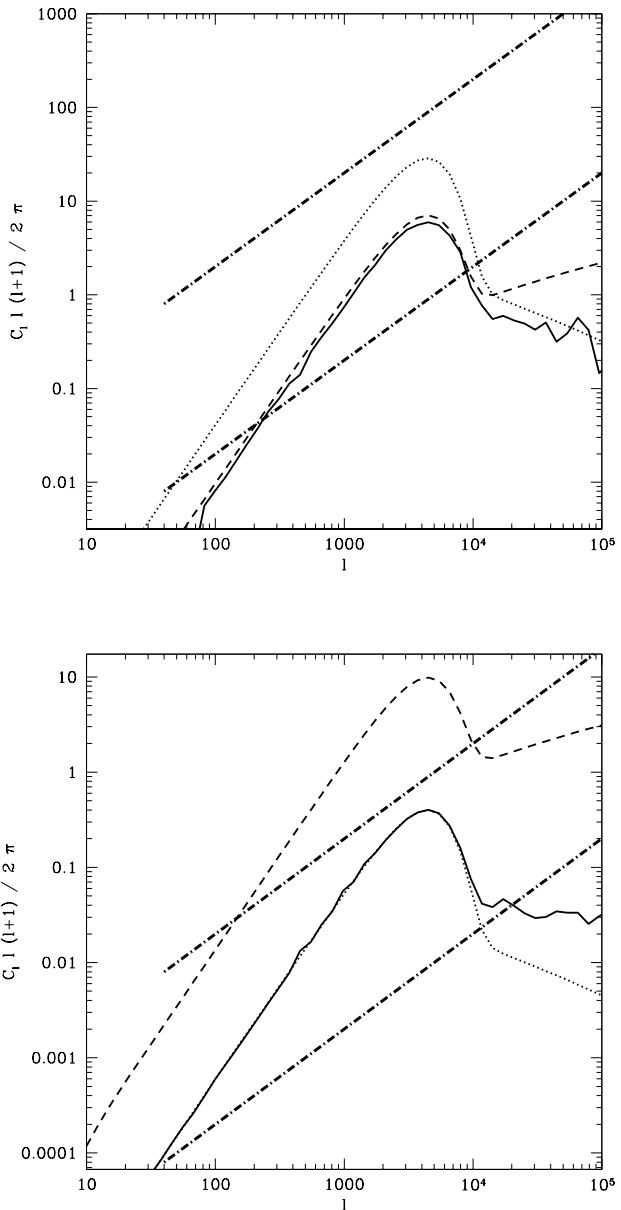


Figure 4. The power spectra calculated for the reionization and bubble model used in this paper at $z = 10$ using three different approximation schemes discussed in the text. Solid line is the full calculation of the equation (8), dashed is the delta-function approximation of equation (39) and dotted line is the Limber approximation of equation (42). The bandwidth of 0.1MHz was used for the top graph and 10MHz for the bottom one. The dot-dashed lines denote the expected $\Delta^{\text{noise}} C_\ell$ for LOFAR and SKA experiments.

the 21-cm signal with the SZ signal. We note that this graphs looks suspiciously similar to the right panel of Figure 6.

These features are easy to understand, if we look at the “source” functions plotted in Figure 8. There we plot the functions which are proportional to the amplitude of the signal given the same power spectrum. We note that particularly for the case of the IR signal, we can clearly

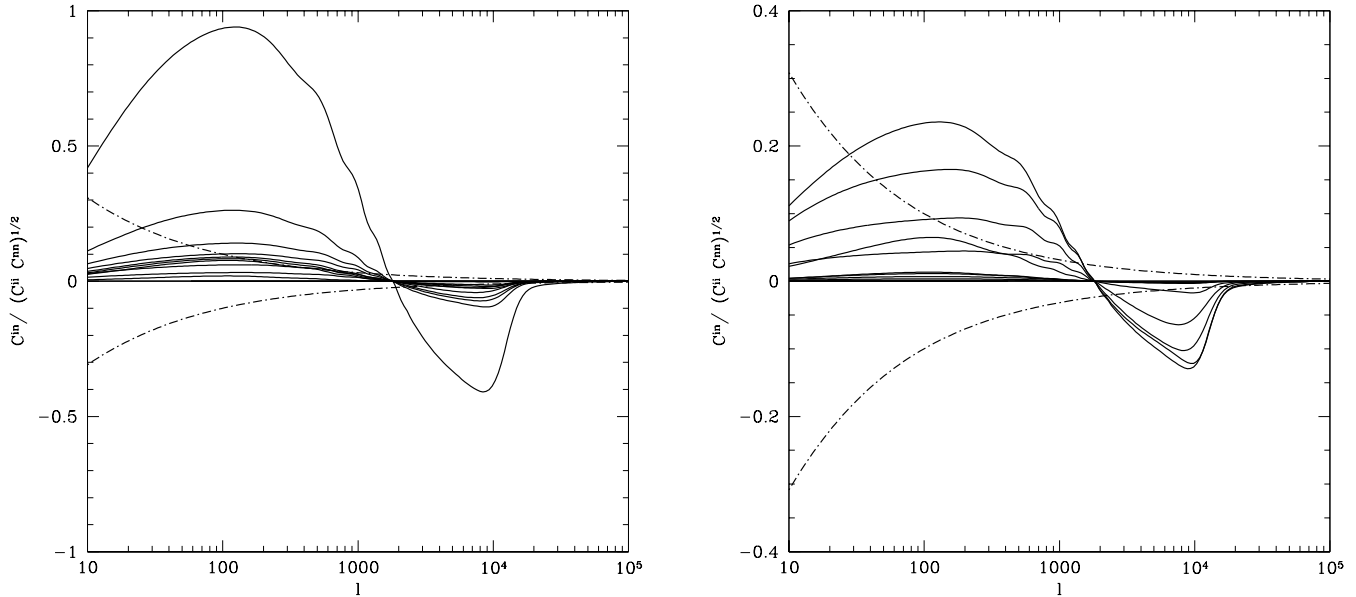


Figure 6. The cross-correlation power spectra for 21-cm anisotropy at redshifts between 8 and 19 correlated against IRB observed at wavelengths of $1.94\mu\text{m}$ (left panel; frequency chosen so that peak occurs at integer redshift, see also Figure 8) and $4\mu\text{m}$ (right panel). The bandwidth of the 21-cm signal was set to 10MHz. The redshift of maximum amplitude is 15 for $1.94\mu\text{m}$ and 11 for $4\mu\text{m}$.

see the features of the spectrum plotted in the Figure 2: If we choose to observe the spectrum at large wavelengths, the spectrum is essentially featureless, while if we choose to observe at $\sim 2\mu\text{m}$ we get the pronounced spike at $z \sim 15$. It is clear from this graph, the the maximum cross-correlation for either SZ or IR signal at $4\mu\text{m}$ should happen at $z \sim 11$, while the IR correlation is nearly completely sourced at $z \sim 15$.

4.1 Observability

Is the signal large enough to be realistically observed by any of the future experiments?

There are two sources of noise present in any attempt to detect cross-correlation between the two fields: the intrinsic noise properties of instruments used and the sample variance that limits our ability to detect correlations due to a finite solid angle of the sky being observed.

The noise power spectrum for the planned future radio telescopes can be, under some simplifying assumptions be written as (Zaldarriaga et al. 2004)

$$\frac{\ell^2 C_\ell^{\text{noise}}}{2\pi} = \frac{T_{\text{sys}}^2 (2\pi)^2}{\delta\nu t_{\text{int}} f_{\text{cover}}^2} \left(\frac{\ell}{\ell_{\text{max}}} \right) \quad (45)$$

where T_{sys} is the system temperature, $\delta\nu$ is the experiment bandwidth, $\delta\nu$ is the experiment bandwidth, t_{int} is the integration time and f_{cover} is the covering fraction. The error on the estimated power spectrum is then given by

$$\Delta^{\text{noise}} C_\ell^{\text{nn}} \sim C_\ell^{\text{noise}} \frac{\ell_{\text{min}}}{\ell} \quad (46)$$

Very similar consideration hold for IR and SZ experi-

ments. The noise power spectrum is given by

$$C_\ell^{\text{noise}} = 4\pi f_{\text{sky}} \frac{\sigma^2}{N_{\text{pix}}}, \quad (47)$$

where f_{sky} is the fraction of sky observed (or being observed by both experiments for cross-correlation studies), N_{pix} is the number of pixel and σ is noise per pixel. The error on the estimated power spectrum is then given by

$$\Delta^{\text{noise}} C_\ell = \sqrt{\frac{2}{f_{\text{sky}}(2\ell+1)}} C_\ell^{\text{noise}} \quad (48)$$

In the Table 1 we list the expected sensitivities for a few experiments. We discuss the following experiments in this paper: Low Frequency Array (LOFAR; Salter et al. 2004)¹, the Square Kilometer Array (SKA; Carilli & Rawlings 2004)², CIBER (Bock et al. 2006)³, AKARI (Matsuhara et al. 2006)⁴ and PLANCK (The Planck Collaboration 2006)⁵.

In Figure 9, we plot predictions for cross-correlation power spectra and the instrumental sensitivities.

However, sample variance is not necessarily a negligible problem in cross-correlation studies or cases with small f_{sky} : only a small part of the IR or SZ light cross-correlates with the relatively narrow-band 21-cm light and so the rest of the IR signal acts as a source of noise. As a crude approximation, we can assume that the skies are normally distributed and

¹ <http://www.lofar.org>

² <http://www.skatelescope.org>

³ <http://physics.ucsd.edu/bkeating/CIBER.html>

⁴ http://www.ir.isas.jaxa.jp/ASTRO-F/Outreach/index_e.html

⁵ <http://www.rssd.esa.int/index.php?project=Planck>

Experiment	Type	$\ell_{\min} - \ell_{\max}$	f_{sky}	$\Delta^{\text{noise}} C_\ell \ell^2 / 2\pi$ at $\ell = 10^3$
LOFAR	21-cm	$\sim 40 - \sim 10^4$	~ 0.5	0.2mK^2
SKA	21-cm	$\sim 40 - \sim 10^4$	~ 0.5	0.002mK^2
CIBER	IR	$\sim 10^3 - \sim 10^4$	4×10^{-4}	$0.004 \text{ (nW/m}^2/\text{sr)}$
AKARI	IR	$\sim 2 - 5 \sim 10^5$	1	$3 \times 10^{-4} \text{ (nW/m}^2/\text{sr)}$
Planck	SZ	$\sim 2 - \sim 6000$	~ 1	$1\mu\text{K}^2$

Table 1. This table lists the expected sensitivities for two 21-cm and one IR and CMB experiments. For 21-cm signal we assumed one month observation and 10MHz bandwidth (taken from (Zaldarriaga et al. 2004)). For the rocket IR experiment, we assumed $1.8\text{nW/m}^2/\text{sr}$ per pixel with pixel size $17''$ and 16 square degrees of observation and for the fictional AKARI FS (full sky) experiment we assumed noise of $11 \mu\text{Jy}$, beam size of 1.46 arc mins, corresponding to the NEP (North Ecliptic Pole) survey, but expanding it from 6 square degrees to full sky. For Planck experiment we assumed full sky observation at 10 arcmin resolution and noise per pixel of $5 \mu\text{K}^2$.

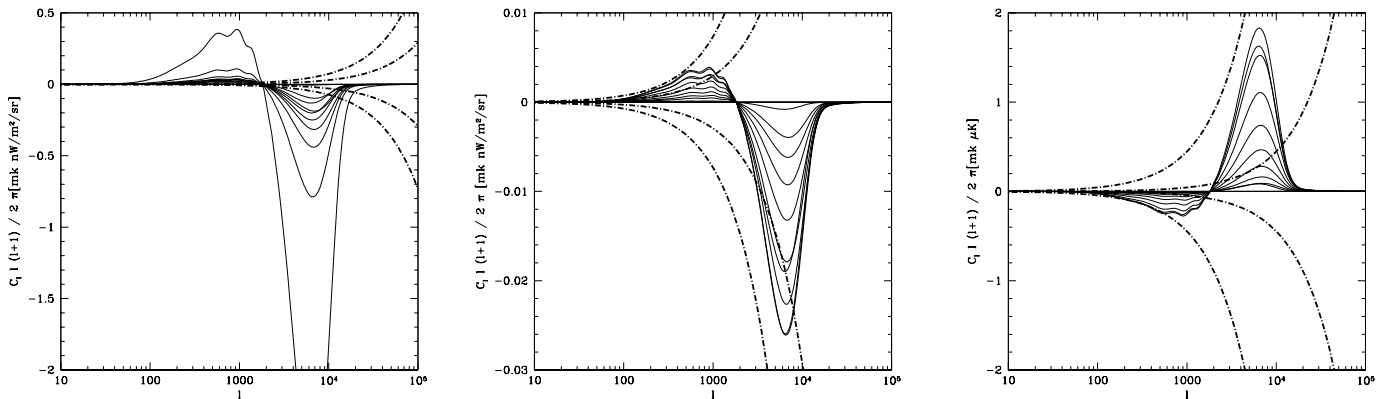


Figure 9. This figure shows the same cross-correlations as in the Figures 6 and 7, but in absolute units. Left and middle panels are for 21-cm-IR cross correlation at $1.94\mu\text{m}$ and $4\mu\text{m}$ respectively, the right panel is for 21-cm-SZ cross-correlation. The expected sensitivities for experiments in Table 1 are also plotted as dashed lines (outer contours are for cross-correlations with LOFAR, inner for cross-correlations with SKA).

so the sample variance errors are given by

$$\Delta^{SV} C_\ell^{xy} = \sqrt{\frac{2C_\ell^{xx} C_\ell^{yy}}{f_{\text{sky}}(2\ell + 1)}}, \quad (49)$$

for $\ell \gg 2$ and the dummy indices x and y are to be replaced with n (21-cm signal), i (IR signal) or y (SZ signal). For $f_{\text{sky}} = 1$ the sample variance is often termed cosmic variance.

This justifies our choice of bandwidth to be 10 MHz. When entering the Limber regime, the 21cm signal drops in amplitude, while the cross-correlation signal stays, to first order, the same. Hence, the cross-correlation is easier to detect if we use wide-bandwidth experiment (or bin the data in a suitable manner). In Figures 6 and 7 we plotted the cosmic-variance limits as a dashed line. At 10MHz they do not seem to be a problem, but they might be at smaller bandwidths. One must also note that these error-bars increase with $f_{\text{sky}}^{-1/2}$, where f_{sky} is the fraction of sky being observed and so this might be a serious problem for experiments that observe only small patches of the sky. Note, however, that these lines correspond to errors per single ℓ : if one combines a range of ℓ values as is usually the case, the error drops correspondingly.

The total error is just the of sample variance error and the noise error added in quadrature:

$$(\Delta^{\text{tot}} C_\ell)^2 = (\Delta^{SV} C_\ell)^2 + (\Delta^{\text{noise}} C_\ell)^2 \quad (50)$$

Which source of error is dominant? In the Figure 10 we plot the ratio of sample variance to noise error on C_ℓ for various auto- and cross- spectra. We note that the sample variance is important in most of the experiments discussed here. This implies that increasing the fraction of the observed sky will improve constraints.

The overall signal-to-noise ratio (SNR) for a given experiment or pair of experiments can be simply calculated by

$$\text{SNR}^2 = \sum_\ell \left(\frac{C_\ell}{\Delta^{\text{tot}} C_\ell} \right)^2, \quad (51)$$

where index ℓ runs over the multipole values for which a given experiment (or both in case of cross-correlation) has coverage. Assuming values from Table 1, we have estimated the total SNR for various experiments. These are given in the Table 2. Note that we chosen $z = 14$ as the target 21-cm redshift. If we chose the redshift corresponding to the peak of the Pop-III spectrum, the SNR values would have been much more favorable.

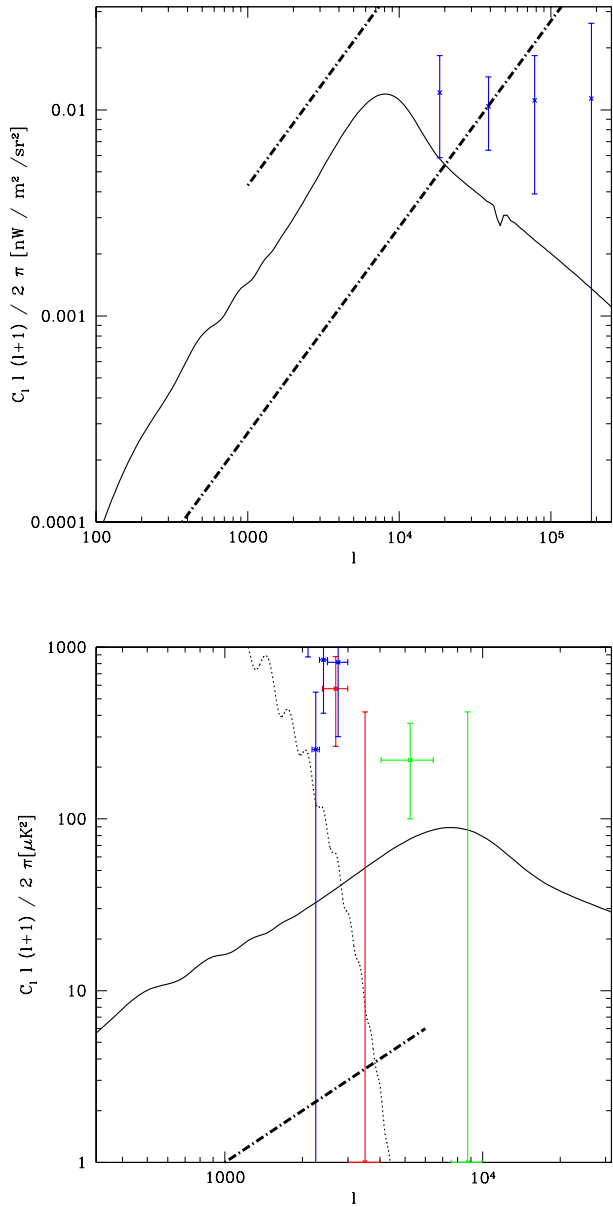


Figure 5. The auto-correlation power spectra contribution from early stars for IR (top) and SZ (bottom). For IR contribution we show the predicted power spectra, the data-points from Kashlinsky with shot-noise contribution subtracted (for details see Sullivan et al. 2006) for details). Straight dot-dashed lines are the expected $\Delta^{\text{noise}} C_\ell$ for the CIBER (top; see (top; for details see Bock et al. 2006) and AKARI (for details see Matsuhara et al. 2006) experiments). For SZ contribution we plot the predicted auto-correlation power spectrum, the data-points from CBI (red), ACBAR (blue) (rescaled by 4.3 to account for different observing frequency of ACBAR assuming that the signal is dominated by the SZ effect) and BIMA (green). The straight dot-dashed line is the expected $\Delta^{\text{noise}} C_\ell$ for the PLANCK experiment.

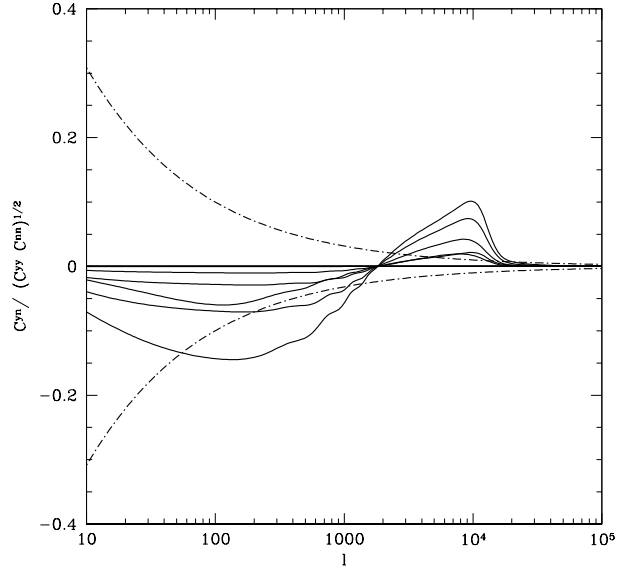


Figure 7. The same as figure 6 but for cross-correlating 21-cm with Comptonization parameter expressed in units of temperature decrement in the Rayleigh-Jeans region of the spectrum.

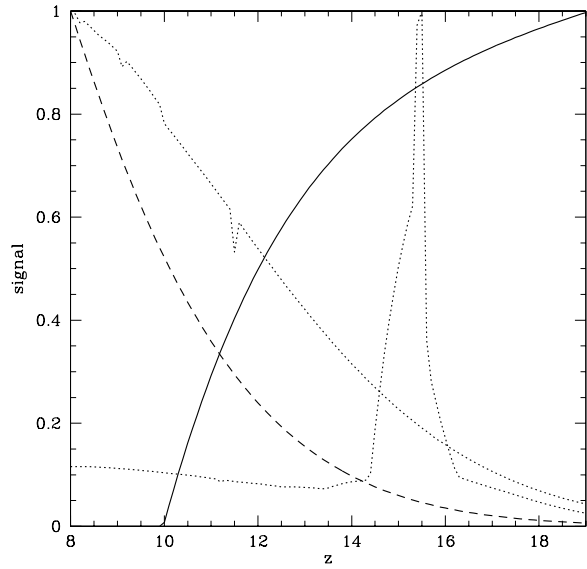


Figure 8. This figure shows the functions that source auto- and cross-correlation power spectra as a function of redshift. We plot $T_0 \bar{\psi}$ (solid line), $dI_\nu/dr\bar{\phi}$ (for $\nu_{\text{obs}} = 2\mu\text{m}$ which has spike at $z \sim 15$ and $\nu_{\text{obs}} = 4\mu\text{m}$; dotted) and $dy/dr\bar{\phi}$. All curves were normalized to unity at maximum.

4.2 Recovering $\bar{x}_H(z)$

From what it was said above, it is clear that there is hope for reconstruction reionization history using cross-correlations discussed here. In Figure 11 we plot the cross-correlation as a function of redshift at $\ell = 6000$ for a number of observing wavelengths. The same plot for SZ-21cm correlations would

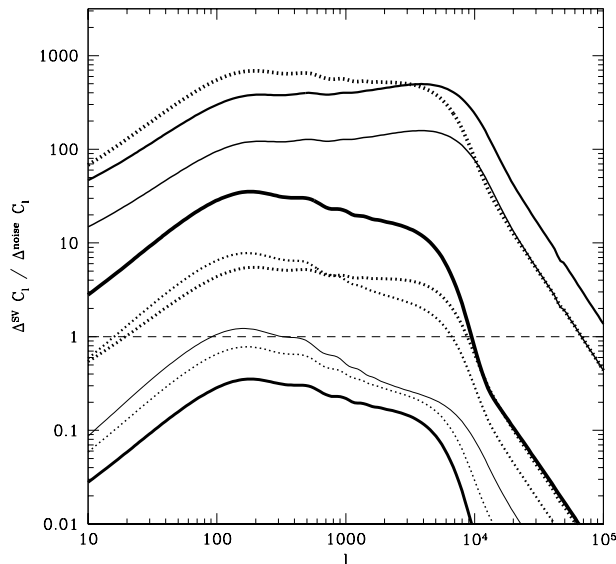


Figure 10. This figure shows the ratio of sample variance to noise error per C_ℓ . The solid lines are for auto-correlations with experiments under consideration are given by line weight: LOFAR (thickest), SKA, CIBER, AKARI, Planck (thinnest). The dotted line are for cross-correlations and we plot the following combinations: LOFAR \times CIBER (thickest), SKA \times AKARI, LOFAR \times Planck, SKA \times AKARI Planck (thinnest).

Experiment	SNR
LOFAR \times LOFAR	~ 250
SKA \times SKA	~ 2000
CIBER \times CIBER	~ 1000
AKARI FS \times AKARI FS	$\sim 4 \times 10^4$
Planck \times Planck	~ 800
LOFAR \times CIBER	~ 40
SKA \times AKARI FS	~ 1300
LOFAR \times Planck	~ 36
SKA \times Planck	~ 137

Table 2. This table lists the expected signal-to-noise ratios for various experiments discussed, assuming the target redshift of $z = 14$ and observing wavelength $\sim 2\mu\text{m}$.

qualitatively very similar to that of the case of observing at $4\mu\text{m}$ or $10\mu\text{m}$. In the same plot we also plot the value of $\bar{x}_H(1 - \bar{x}_H)(z/11)^2$.

It is clear from the plot that one can, if one observes at the right wavelength, in principle constrain $\bar{x}_H(1 - \bar{x}_H)$ and therefore the neutral fraction as a function of time. We will not go into details of feasibility as there are many theoretical details that needs to be worked out, in particular the details of star-formation, spectral features, bubble size, etc.: difficult problems, which should be nonetheless solved by more detailed modeling. We also note, that there are several spectra: many degeneracies can be broken by, for example, using auto-correlation spectra to recover star-formation histories, etc.

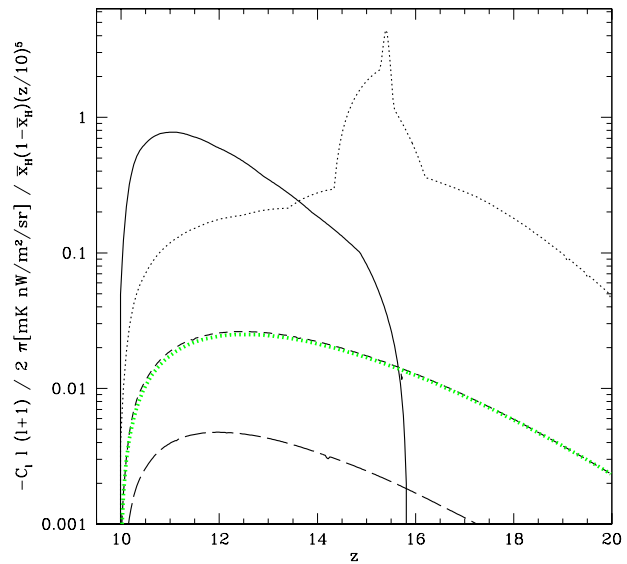


Figure 11. This figure shows the cross-correlation power spectra at $\ell = 6000$ as function of target for IR observing wavelengths of $1\mu\text{m}$ (solid), $2\mu\text{m}$ (dotted), $4\mu\text{m}$ (dashed) and $10\mu\text{m}$ (long dashed). The thick green dotted line in the plot of $\bar{x}_H(1 - \bar{x}_H)(z/11)^2$

5 DISCUSSION AND CONCLUSIONS

In this paper we have presented a simple model for auto- and cross-correlations of the 21-cm, IR and SZ signals from the first stars. In particular, the cross-correlations of 21-cm signal with either IR or SZ signals as a tool to measure reionization history was introduced for the first time.

The cross-correlation power spectra have a distinct shape: on scales smaller than the bubble size the anti-correlate, because stars and supernovae glow in negative with respect to the 21-cm sky. On large scales, they both trace density fluctuations and correlate positively.

Cross-correlations have the usual advantage over auto-correlations in that foregrounds automatically cancel, unless foregrounds for two signals also cross-correlate, which is unlikely due to a very different nature of foregrounds for the signals discussed in this paper. A realistic possibility are radio-galaxy/AGN that can be seen both in radio through synchrotron emission and in the infrared by the dust emission. Di Matteo et al. (2004) have argued that if bright sources are removed above flux levels of $S \gtrsim 0.1\text{mJy}$ the *auto*-correlation power spectra should be uncontaminated for $\ell \lesssim 10^4$ and only contaminated at $O(1)$ for $\ell \gtrsim 10^4$. One could argue that something similar holds for the cross-correlation. If significant, one could model this cross-correlation and add it to the model: note that the sign of cross-correlation is different on small scales and hence this cannot produce a false detection. Finally, one could resort to using spectral cleaning techniques (Morales et al. 2006), although this would defy one of the main advantages of cross-correlation.

We have shown that the tomography of cross-correlations of 21-cm signal with the IR and SZ signal has,

in principle, potential to strongly constrain the reionization, especially in the region when $\bar{x}_H \sim 0.5$. When observed at smaller IR wavelengths, the cross-correlation actually traces the spectrum of the primordial stars and strong features, such as Lyman-alpha peak could be clearly reconstructed from the data.

We have roughly modeled the noise properties of several up-coming experiments. Detection properties of experiments to detect cross-correlations is often limited by a limited fraction of sky observed with the first-generation of experiments. Nevertheless, we predict that detection is within the reach of the next-generation experiments. The most problematic at the moment is the IR field: the early experiments such as CIBER or the AKARI NEP (North Ecliptic Pole) survey are simply limited by a small fraction of the sky being observed. A full-sky map at the sensitivity of AKARI NEP, will be clearly able to detect the cross-correlation. We note, that the signal-to-noise ratios given in the Table 2 are for a single 21-cm signal cross-correlation: stacking many of them will, of course, improve the signal-to-noise ratio accordingly.

Finally, we note that our model is overly simplistic in many aspects. Firstly, we assume a continuous Pop-III star-formation together with continuous production of massive supernovae. In reality, however, massive supernovae will pollute their environment with metals and hence quench the Pop-III star formation, leading to a fast transition to the Pop-II stars. Alternatively, supernovae are not so energetic and Pop-III stars can actually completely reionize the Universe. In the former case, our high-redshift calculations still hold, but at lower redshifts both IR and SZ cross-correlations disappear as both Pop-II star-light and the corresponding supernovae are much less energetic. In the latter case, IR correlates with 21-cm throughout the duration of reionization, but we overestimated cross-correlation with SZ. In either case, the cross-correlations can be used to constrain reionization process. Secondly, the constant bubble-size used here cannot hold. In reality, the bubble size increases and gets to the level of few Mpc at the peak of the reionization process, when $x_H \sim 0.5$ and the bubbles have not merged yet. Latter the bubbles merge and the bubble-size is not a well-defined quantity. In this work we used $4 h^{-1}$ Mpc for a typical size of bubble and $2h^{-1}$ Mpc for the typical size of sources. Lowering the size of sources pushes the auto-correlation and cross-correlation spectra up. However, the relative amplitudes decreases and hence the prospects for detection decrease. Thirdly, the cross-correlation terms between the neutral fraction and the density were ignored in this work, following the analysis in Zaldarriaga et al. (2004). While these terms might be important, it is not immediately clear what would their effect be. An analytical model for cross-correlation has been developed in Furlanetto et al. (2004) and the study of this effect is deferred to a forthcoming publication.

In this paper we have put forward a novel idea for extracting information of reionization. Adding details to the model, such as bubble size growth, neutral fraction – density correlation, etc., either through a more accurate analytical modeling, but probably more likely through insight from numerical codes, will probably improve and somewhat change predictions presented here, but hopefully only at the quantitative level.

ACKNOWLEDGMENTS

AS is supported by Oxford Astrophysics. AC thanks Peng Oh for useful discussions.

REFERENCES

- Alvarez M. A., Komatsu E., Dore O., Shapiro P. R., 2006, *ApJ*, 647, 840
 Barkana R., Loeb A., 2001, *Phys. Rept.*, 349, 125
 Bock J. et al., 2006, *New Astronomy Review*, 50, 215
 Cambr esy L., Reach W. T., Beichman C. A., Jarrett T. H., 2001, *ApJ*, 555, 563
 Carilli C., Rawlings S., 2004, *ArXiv Astrophysics e-prints*
 Cen R., 2003a, *Astrophys. J.*, 597, L13
 Cen R., 2003b, *Astrophys. J.*, 591, 12
 Cohn J. D., Chang T.-C., 2006, *ArXiv Astrophysics e-prints*
 Cooray A., others , 2006
 Cooray A., Bock J. J., Keating B., Lange A. E., Matsumoto T., 2004, *Astrophys. J.*, 606, 611
 Cooray A. R., Yoshida N., 2004, *Mon. Not. Roy. Astron. Soc.*, 351, L71
 Dawson K. S., Holzzapfel W. L., Carlstrom J. E., Joy M., LaRoque S. J., 2006, *ApJ*, 647, 13
 Dawson K. S., Holzzapfel W. L., Carlstrom J. E., Joy M., LaRoque S. J., Miller A. D., Nagai D., 2002, *ApJ*, 581, 86
 Di Matteo T., Ciardi B., Miniati F., 2004, *MNRAS*, 355, 1053
 Fernandez E., Komatsu E., 2006, *Astrophys. J.*, 646, 703
 Furlanetto S., Lidz A., 2006, *ArXiv Astrophysics e-print*
 Furlanetto S., Sokasian A., Hernquist L., 2004, *Mon. Not. Roy. Astron. Soc.*, 347, 187
 Furlanetto S., Zaldarriaga M., Hernquist L., 2004, *Astrophys. J.*, 613, 1
 Furlanetto S. R., Oh S. P., 2005, *MNRAS*, 363, 1031
 Furlanetto S. R., Oh S. P., Briggs F. H., 2006, *Phys. Rep.*, 433, 181
 Furlanetto S. R., Zaldarriaga M., Hernquist L., 2004, *ApJ*, 613, 16
 Haiman Z., Holder G. P., 2003, *Astrophys. J.*, 595, 1
 Hauser M. G., Dwek E., 2001, *ARA&A*, 39, 249
 Iliev I. T., others , 2006a, *Mon. Not. Roy. Astron. Soc.*, 369, 1625
 Iliev I. T., Mellema G., Shapiro P. R., Pen U.-L., 2006b
 Kashlinsky A., 2006, *New Astron. Rev.*, 50, 208
 Kashlinsky A., Arendt R., Gardner J. P., Mather J. C., Moseley S. H., 2004, *Astrophys. J.*, 608, 1
 Kashlinsky A., Arendt R. G., Mather J. C., Moseley S. H., 2005, *Nature*, 438, 45
 Kohler K., Gnedin N. Y., Hamilton A. J. S., 2005
 Kuo C.-L., others , 2006, *ArXiv astro-ph/0611198*
 Kuo C. L. et al., 2004, *ApJ*, 600, 32
 Mackey J., Bromm V., Hernquist L., 2003, *Astrophys. J.*, 586, 1
 Madau P., Haardt F., Rees M. J., 1999, *Astrophys. J.*, 514, 648
 Madau P., Meiksin A., Rees M. J., 1997, *Astrophys. J.*, 475, 429
 Madau P., Silk J., 2005, *Mon. Not. Roy. Astron. Soc.*, 359, L37

- Mason B. S. et al., 2003, *ApJ*, 591, 540
Mather J. C. et al., 1994, *ApJ*, 420, 439
Matsuhara H., others , 2006, *Publ. Astron. Soc. Jap.*, 58, 4
Matsumoto T., others , 2005, *Astrophys. J.*, 626, 31
McQuinn M., Furlanetto S. R., Hernquist L., Zahn O., Zaldarriaga M., 2006, *New Astronomy Review*, 50, 84
McQuinn M., Zahn O., Zaldarriaga M., Hernquist L., Furlanetto S. R., 2005, *ArXiv Astrophysics e-prints*
Mellema G., Iliev I. T., Pen U.-L., Shapiro P. R., 2006, *Mon. Not. Roy. Astron. Soc.*, 372, 679
Mo H. J., White S. D. M., 1996, *MNRAS*, 282, 347
Morales M. F., Bowman J. D., Hewitt J. N., 2006, *ApJ*, 648, 767
Oh S. P., 2001, *ApJ*, 553, 499
Oh S. P., Cooray A., Kamionkowski M., 2003, *Mon. Not. Roy. Astron. Soc.*, 342, L20
Press W. H., Schechter P., 1974, *ApJ*, 187, 425
Salter D. M., Paardekoooper J.-P., Röttgering H. J. A., Bähren L., Brentjens M., Falcke H., Wijnholds S., 2004, in *Bulletin of the American Astronomical Society*
Salvaterra R., Ferrara A., 2003, *Mon. Not. Roy. Astron. Soc.*, 339, 973
Salvaterra R., Ferrara A., 2006, *Mon. Not. Roy. Astron. Soc. Lett.*, 367, L11
Salvaterra R., Magliocchetti M., Ferrara A., Schneider R., 2006, *Mon. Not. Roy. Astron. Soc. Lett.*, 368, L6
Santos M. G., Cooray A., 2006, *Phys. Rev.*, D74, 083517
Santos M. G., Cooray A., Haiman Z., Knox L., Ma C.-P., 2003, *Astrophys. J.*, 598, 756
Santos M. G., Cooray A., Knox L., 2005, *Astrophys. J.*, 625, 575
Santos M. R., Bromm V., Kamionkowski M., 2002, *Mon. Not. Roy. Astron. Soc.*, 336, 1082
Scott D., Rees M. J., 1990, *MNRAS*, 247, 510
Sullivan I., others , 2006, *ArXiv Astrophysics e-prints*
The Planck Collaboration , 2006, *ArXiv Astrophysics e-prints*
Tozzi P., Madau P., Meiksin A., Rees M. J., 2000, *ApJ*, 528, 597
Venkatesan A., Giroux M. L., Shull J. M., 2001, *ApJ*, 563, 1
Wyithe J. S. B., Loeb A., 2003, *ApJ*, 588, L69
Wyithe S., Loeb A., 2006, *ArXiv e-prints*, astro-ph/0609734
Yoshida N., Abel T., Hernquist L., Sugiyama N., 2003, *Astrophys. J.*, 592, 645
Yoshida N., Bromm V., Hernquist L., 2004, *Astrophys. J.*, 605, 579
Zahn O., Lidz A., McQuinn M., Dutta S., Hernquist L., Zaldarriaga M., Furlanetto S. R., 2006, *ArXiv Astrophysics e-prints*
Zahn O., Zaldarriaga M., Hernquist L., McQuinn M., 2005, *ApJ*, 630, 657
Zaldarriaga M., Furlanetto S. R., Hernquist L., 2004, *Astrophys. J.*, 608, 622